Letter | Featured in Physics

Insight into the Design and Fabrication of a Leaf-Mimicking Micropump

Prashant Agrawal,[1] Prasanna S. Gandhi,[2] Mainak Majumder,[3] and Prasoon Kumar[4,*]

[1] *Smart Materials and Surfaces Laboratory, Faculty of Engineering and Environment, Northumbria University, Newcastle upon Tyne, NE1 8ST, United Kingdom*

[2] *Suman Mashruwala Advanced Microengineering Laboratory, Department of Mechanical Engineering, Indian Institute of Technology Bombay, Powai, Mumbai, Maharashtra 400076, India*

[3] *Nanoscale Science and Engineering Laboratory (NSEL), Department of Mechanical and Aerospace Engineering, Monash University, Clayton, Melbourne, Australia*

[4] *Department of Medical Devices, National Institute of Pharmaceutical Education and Research Ahmedabad, Gandhinagar, Gujarat, India*

(Received 19 June 2019; published 20 September 2019)

A micropump is the heart of any microfluidic device that finds applications in several lab-on-chip devices. Passive micropumps are highly desirable for this purpose due to their ease of integration, low energy requirements, and simplistic design and operation. The design of a plant leaf serves as natural inspiration for the development of an evaporation-assisted passive micropump. The presence of a branching-channel-like venation pattern ensures water distribution to the spongy mesophyll cells, increasing the surface area for evaporation. However, because of its multiscale design and the complexity of the venation pattern, emulating a leaf's design is challenging. Apart from the lack of understanding of design parameters that affect fluid flow, manufacturing limitations impede the development of such bioinspired micropumps. Inspired by the multiscale design of the leaf, in this work we propose a passive micropump mimicking the structure of a leaf. Using evaporation and capillary pressure as the pumping mechanism, our leaf-mimicking micropump consists of a microporous membrane integrated with a branched, fractal channel network resembling a leaf's venation pattern. Our proposed fabrication method is simple, scalable, and inexpensive and uses readily available materials. We demonstrate a significant increase in the fluid flow rate due to the addition of this branched-channel network. We support our experimental observations using an analytical model, wherein we discuss the design parameters that affect the pumping rate. Correspondingly, the performance of these micropumps can be optimized on the basis of intrinsic and extrinsic factors as per the desired applications.

DOI: 10.1103/PhysRevApplied.12.031002

Micropumps form an integral part of many microfluidic systems where precise control over fluid delivery is required. Such controlled delivery is desirable in applications such as advanced drug-delivery systems, lab-on-chip devices, and microelectronic cooling systems [1–3]. Passive micropumps offer promising solutions as they can circumvent problems posed by active micropumps [4–6], such as energy consumption, actuation mechanism integration, and oscillating or pulsating flows. Toward the development of such passive micropumps, tree leaves in nature serve as inspiration for evaporation-assisted passive micropumping for microfluidic applications [7].

Several studies have looked at developing artificial leaf systems focusing either on the use of novel materials [8–10] or device design to increase the surface area of evaporation [11–13]. Hydrogels have recently been proposed as a material for water storage and imbibition applications [14]. The low chemical potential of water in hydrogels imparts high mobility to water molecules, which allows large pressure heads for wicking water [15]. Such hydrogels can simultaneously function as a tree trunk (for water transportation) and as a leaf (for evaporation) [14]. Hydrogels can also be combined with microporous membranes to control the evaporative flux on the basis of the pore size [13]. Additional designs include mimicking the functional and structural form of a leaf's stomata with slitlike micropores [16]. With use of thermoresponsive polymers, these micropores can be actuated to emulate the closure of a leaf's stomata with variation in temperature, thereby controlling the pumping rate [17].

Although hydrogels provide high-pressure heads, they are structurally weak materials, and are less suitable in applications demanding structural support and relatively high flow rates [18]. As an alternative, microporous substrates have been used to provide structural

*prasoonkumar1985@gmail.com

stability with relative ease of fabrication. In these substrates the capillary pressure in the pores of the substrate provides the necessary pressure head for pumping. Therefore, the flow rate primarily depends on the material and size of the pores, which also dictates the available evaporative surface area [19]. Here the length and diameter of the channel irrigating the substrate (analogous to a tree trunk) do not alter the pumping rate significantly [19]. However, by incorporation of a multichannel pattern that irrigates the substrate, the net evaporative flux can be greatly enhanced [20]. Here the density and shape of the pattern are crucial in lowering the flow resistance and increasing the evaporative surface area. Previous studies primarily used parallel arrays of rectangular channels to mimic this venation pattern as fabricating a three-dimensional multiscale branching channel is complex and relies on expensive lithographic processes [21]. Furthermore, the parallel-channel designs are not necessarily optimized for lowering the fluid-flow resistance.

Therefore, in the present work, we propose an alternative design of a passive micropump that mimics the venation pattern of a leaf using a simple, inexpensive, and scalable fabrication method (depicted in Fig. 1). The leaf-mimicking micropump (LMM) comprises radially arranged, three-dimensional, branch-shaped, multiscale microchannels (representing leaf veins) integrated into a microporous substrate (resembling stomata and spongy mesophyll cells). We compare the evaporative flow rate obtained in the LMM with that obtained in a control substrate devoid of the venation pattern. The LMM demonstrates enhanced flow rates compared with similar microporous-membrane-based passive micropumps. Furthermore, we use an analytical model to validate and explain the performance of the micropumps. The model agrees with experimental results and can serve as a design guide for fabricating such bioinspired micropumps for specific applications.

The fabrication process for the LMM is shown in Fig. 1(c). The fractal microchannel network is obtained with use of a bespoke Hele-Shaw apparatus based on Saffman-Taylor instabilities [22]. A thoroughly mixed ceramic suspension, consisting of alumina particles (0.5 μm) added to 1,6-hexanediol diacrylate monomer with benzoin ethyl ether and phosphate ester, as per the process developed by Adake *et al.* [23], is used to create the mold for the channel network. The channel network obtained from the Hele-Shaw apparatus (overall diameter 30 mm) is heated over a hot plate at 120°C for 24 h to cure and form a stable mold ready for casting. After curing, polydimethylsiloxane (PDMS) (Sylgard 184; elastomer:curing agent weight ratio 10:1) is poured over the mold and cured over a hot plate at 80°C for 6 h. The cured PDMS (thickness approximately 2 mm) is peeled off to form the open fractal microchannel network. The hydraulic diameter of the channels so obtained decreases from the parent to the final, fourth-generation branch [shown as channel width and height in Figs. 1(d) and 1(v)] [24].

To integrate the channel network with a microporous substrate, PDMS is spin coated at 800 revolutions/min for 2–3 min on paraffin wax paper and left at room temperature for 24 h for partial curing. This partially cured PDMS film is then placed on microporous filter paper (Whatman, 90-mm diameter) and the film and filter paper are bonded together by heating at 100°C for 15 s. Thereafter, the paraffin wax paper is removed and the cured fractal channel network substrate is pressed on the exposed side of the PDMS film, which is adhered to the microporous substrate on the other side. The entire device is then heated at 60°C for 1.5 h to cure the PDMS film and strengthen the bonding between the channel substrate and the microporous filter paper. The diameter of the bonding PDMS film is such that the terminal ends of the channel network are in contact with the microporous substrate.

The fabricated LMM is placed on a stage [depicted in Fig. 1(d)] such that the outer part of the substrate is exposed for evaporation. The LMM is connected to one end of a polytetrafluoroethylene (PTFE) tube (length 790 mm and internal diameter 2 mm), while the other end of the tube is placed in a reservoir. Initially, the reservoir and

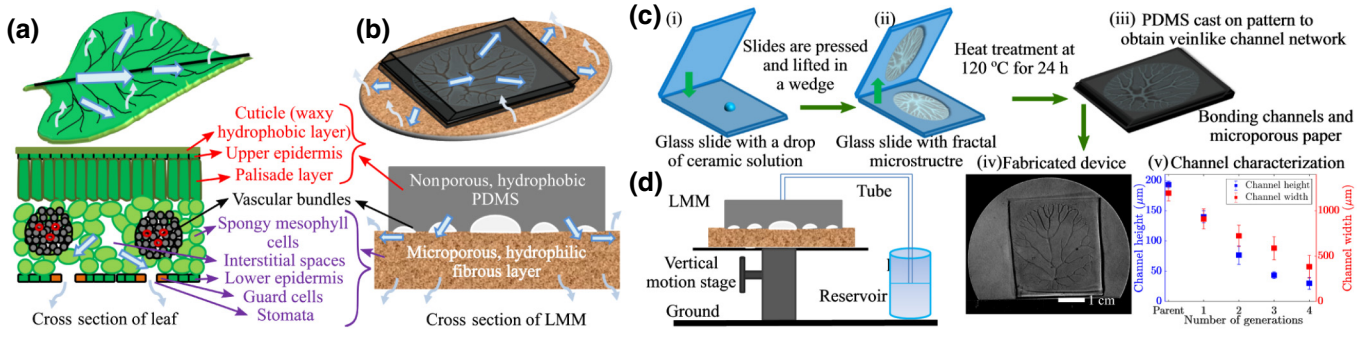

FIG. 1. The concept of a leaf-mimicking micropump (LMM): (a) the macrostructure and microstructure of the leaf; (b) analogous LMM structure; (c) fabrication procedure for the LMM (i)–(iv), showing the final device (iv) and channel sizes (v); (d) experimental setup for measuring the flow rate from the LMM at different pressure heads.

the LMM are placed at the same level from the ground. The reservoir is then slowly raised above the LMM by 2 mm to enable water to flow through the tube to the microporous substrate. The flow of water is continued until the entire microporous substrate is saturated. This preconditioning is necessary to avoid the effect of water absorption by the dry substrate on the measured flow rates. Next, the reservoir is lowered down to the level of the LMM and is left for 15 min to reach the steady state. In this steady state, the volumetric flow through the microporous substrate is equal to the evaporative flux of water from the exposed surface of the substrate. Next, an air bubble is introduced in the tube from the end placed in the reservoir. The LMM is left in open air in a clean-room environment at 25°C and relative humidity of 50%. Evaporation will produce relatively higher humidity (than ambient) around the substrate area and will induce evaporative cooling on the substrate, which might affect evaporation. However, the local temperature and humidity were not monitored during experiments, as they are inherently accounted for in the pumping performance. Furthermore, air flow over the substrate can significantly affect the evaporation rate. Although no controlled air flow was used, air currents due to experimenter's movement and room ventilation might affect the pumping rate and could be a source of deviation in the observed data. The pumping speed is measured by tracking the position of the air bubble in the tube. To assess the pressure head generated by the LMM, the LMM is raised in steps and allowed to stabilize for 15 min at each step before the air bubble is tracked. The process of raising the LMM ceases when there is no appreciable change in the position of the air bubble. Control experiments are performed with a device wherein a PTFE tube (of the same length) is connected directly to the microporous substrate without any intermediate microchannel network.

The flow rates obtained from the LMM and the control device are shown in Fig. 2. At zero pressure head ($h = 0$ mm), the average liquid pumping rate ($\dot{M}_e$) of the LMM is about 0.108 mg/s, which is approximately

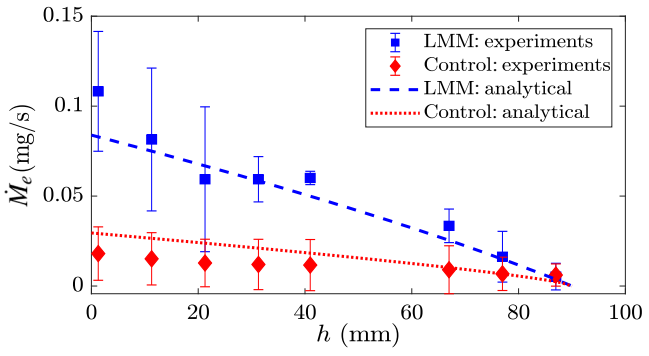

FIG. 2. Experimental results of mass flow rate against LMM height. The dashed and dotted lines represent the trend for the LMM [Eq. (3)] and the control setup [Eq. (4)], respectively.

10 times higher than that of the control device ($\dot{M}_e \approx 0.018$ mg/s). In this LMM design, the increased evaporative pumping rate is obtained by enhancing the surface area available for evaporation. The presence of the fractal channel network eases the delivery of the liquid to multiple radially distributed locations on the substrate. These multiple irrigation points increase the radial spread of the liquid as it is imbibed into the microporous substrate. In the absence of this fractal channel network, as in the control device, the pores of the microporous substrate offer a relatively higher resistance to liquid flow for the same spreading area as in the LMM. This higher flow resistance results in a smaller radial spread and, hence, reduced evaporative pumping rates. Therefore, the integration of the fractal channel network effectively reduces the net resistance to the liquid flow, leading to a larger surface area available for evaporation.

Next, by changing the height of the LMM with respect to the reservoir, we look at the variation of the mass flow rate with pressure head. We observe that the liquid pumping rate of the LMM declines approximately 10 times faster than that of the control microporous substrate (Fig. 2). As the height is increased, bubbles are observed around the terminal ends of the channel network at around 40 mm. This bubble entrainment is a limitation of the fabrication process that can be overcome by improving the contact between the terminal ends of the channel with the microporous substrate. With further increase in height, these bubbles nucleate and migrate toward the tube connecting the reservoir to the LMM. Above a height of approximately 85 mm, the capillary pressure in the substrate is unable to sustain the flow, wherein air bubbles completely block the terminal ends of the channel network and prevent liquid flow.

To investigate the difference in the behavior of the LMM and the control substrate, we analytically model the evaporation rate as a function of the LMM height. At steady state, the continuous pumping is driven by evaporation from the exposed area of the microporous substrate. This flow is resisted by the gravitational pressure head introduced by our raising the LMM and the viscous friction from the flow in the porous substrate, the channel network, and the tubing connecting the LMM to the liquid source. We assume that the terminal ends of the fractal channel form a continuous ringlike liquid source and adopt the model developed by Liu *et al.* [25]. At steady state, the flow in the porous substrate is described by [24]

$$P_c' = \frac{\mu \dot{m}_e R_0^2}{4K\rho H}(1 - x + x\log x), \tag{1}$$

where $\dot{m}_e$ is the rate of evaporation per unit area from the surface (assumed to be constant under the same atmospheric conditions and for the same substrate type), K is the permeability and H is the thickness of the porous

substrate, ρ and μ are the density and the viscosity of the liquid, R_0 is the radius of the liquid source, and $x = R^2/R_0^2$, where R is the radius of the wetted region. Because of the ringlike configuration of the liquid source, there are two solutions of x, corresponding to $R_{\max} \subseteq R > R_0$ and $R_{\min} \subseteq R < R_0$. However, considering the substrate orientation in the experiments, we consider only one solution of x for comparison with experiments: $x = R_{\max}/R_0$. P_c' is the modified capillary pressure driving the imbibition, accounting for the gravitational pressure head (P_g) and the viscous pressure losses in the fractal channel (P_{vf}) and the tube from the reservoir to the leaf (P_{vt}): $P_c' = P_c - P_{vf} - P_{vt} - P_g$, where, P_c is the capillary pressure in the microporous substrate [26]. The total evaporative mass flux ($\dot{M}_e$) is written as $\dot{M}_e = \dot{m}_e\pi(R_{\max}^2 - R_0^2)$. Equation (1) can be rewritten as

$$\frac{P_c - \rho g h}{c_e \dot{m}_e R_0^2} = x\log x + \left(\frac{c_v}{c_e} - 1\right)(x-1), \qquad (2)$$

where h is the height of the micropump above the reservoir and $c_v = c_{vt} + c_{vf}$, where c_{vt} and c_{vf} represent the coefficient of fluid-flow resistance due to viscous friction in the tube [27] and the fractal channel [28], respectively. Thus, c_v represents the coefficient of fluid-flow resistance due to viscous friction in the macrochannels, while c_e represents the resistance to flow in the microporous substrate. Obtaining accurate values of flow parameters for the microporous substrate is challenging as the permeability estimation is highly dependent on the environmental and setup configurations [29,30]. Therefore, we use approximate analytical values to estimate the relative magnitude of the coefficients [24]. We obtain $c_v/c_e \approx 1$ for the LMM and $c_v/c_e \ll 1$ for the control sample. Therefore, for the LMM, Eq. (2) is rewritten as

$$\frac{P_c - \rho g h}{c_e \dot{m}_e R_0^2} = x\log x, \qquad (3)$$

while for the control sample ($c_v/c_e \ll 1$) Eq. (2) is rewritten as

$$\frac{P_c - \rho g h}{c_e \dot{m}_e R_0^2} = x\log x - (x-1). \qquad (4)$$

The above equations are solved for x to obtain the spreading area and, therefore, the evaporation rate [$\dot{M}_e = \dot{m}_e\pi R_0^2(x-1)$] against h, assuming P_c corresponds to the pressure at $h_{\max} = 85$ mm. As the values used in the analytical model are estimates, we compare the evaporation rates with experimental values by adding a scaling factor (approximately 0.03). This adjustment informs the variation of mass flow rate with height, as opposed to exact numerical values. We see in Fig. 2 that the trends for the LMM and the control sample agree with the experimental observations, affirming the validity of the modeling procedure.

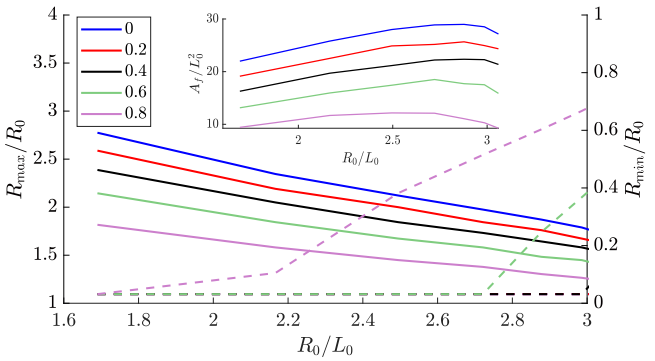

FIG. 3. Variation of wetted area with R_0/L_0 for different gravitational-pressure-head ratios ($h/h_{\max}$), where L_0 is the length of the parent fractal branch. The solid lines correspond to the left y axis and the dashed lines correspond to the right y axis. The inset shows the variation of the evaporative surface area for different pressure-head ratios.

The model can be used to optimize the design of the LMM for different gravitational pressure heads. Considering evaporation from the entire surface of the LMM, Fig. 3 shows the complete solution of Eq. (1) (for $R_{\max}$ and $R_{\min}$) for different source radii (R_0); the source radius here is varied by changing the number of generations of the fractal channel network. A change in the pressure head alters both the outer wetting radius and the inner wetting radius of the substrate, which affect the wetted area and, therefore, the flow rate. For small gravitational pressure heads, the inner surface of the LMM is completely wetted ($R_{\min} = 0$). However, for higher gravitational heads, the suction pressure is insufficient to wet the inner area of the substrate completely ($0 < R_{\min} < R_0$), where $R_{\min}$ depends on R_0 as seen in Fig. 3. The inset shows a maximum evaporative area (A_f) for all pressure heads, which is at around three to five generations of the fractal channel network. The model thus informs device design, where $R_{\max}$ provides the maximum device size, while $R_{\min}$ can be reduced to optimize the wetted area.

The evaporative capacity of any device can be broadly characterized on the basis of two factors: material properties and device design. Using the analogy of hydraulic circuits, we can write the volume flow rate as $Q = \Delta P/R_h$, where ΔP is the pressure gradient (suction pressure) and R_h is the hydraulic resistance. This expression allows us to compare the performance of the LMM with that of previously reported passive micropumps in Fig. 4, where ΔP represents the material properties (pore size, water potential), while Q incorporates information about substrate texture and evaporative area (assuming similar environmental conditions).

The flow rate obtained from the LMM is comparatively similar to that observed in some other reported passive devices, despite a relatively low suction pressure. However, Fig. 4 does not present a complete and fair

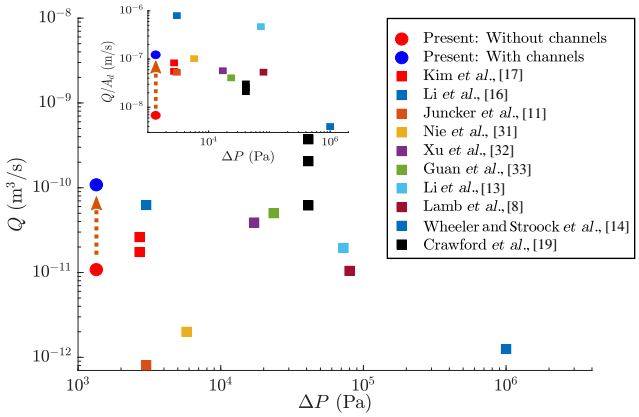

FIG. 4. Comparison of the LMM performance with performances reported in previous studies [8,11,13,14,16,17,19,31–33]: volumetric flow rate (flow rate per unit area in the inset) against suction pressure.

comparison as some of the examples use device sizes designed for specific applications and not necessarily for assessing the performance limit of their designs (apart from Crawford *et al.* [19]). Although the inset in Fig. 4 negates the influence of device size by plotting the flow rate per unit device area, the comparison does not differentiate between completely wetted and partially wetted substrates. Nevertheless, we can see that due to the addition of the venation pattern, the flow rate increases for the same suction pressure. A similar flow-rate enhancement can be obtained if such a venation pattern is included in other designs with a higher suction pressure.

In this work we demonstrate the working of a leaf-inspired passive micropump. The uniqueness of the pump lies in the branched-channel network that irrigates the microporous substrate to increase the evaporative surface area, which significantly enhances the pumping rate. Our manufacturing process provides a simple, inexpensive, and scalable method for fabricating a multiscale branched-channel network (like veins of a leaf), and its integration with any microporous membrane. Analytical modeling of the flow suggests an ideal branching venation pattern for different pressure heads that decreases the overall hydraulic resistance to flow and maximizes the utilization of the substrate surface area during the evaporation process. Therefore, our model and fabrication process can be used as a design template for developing passive micropumps using different substrates (microporous membrane or gel based) for operation in different environmental conditions.

ACKNOWLEDGMENTS

The authors acknowledge IITB-Monash Research Academy for providing financial assistance to carry out this project.

[1] D. J. Laser and J. G. Santiago, A review of micropumps, J. Micromech. Microeng. **14**, R35 (2004).
[2] N. Goedecke, J. Eijkel, and A. Manz, Evaporation driven pumping for chromatography application, Lab Chip **2**, 219 (2002).
[3] D. Daniel, A. Mosyak, R. Akhvlediani, A. Hoffman, and G. Yossifon, Enhanced Cooling of Electronic Chips Using Combined Diamond Coating and Micro Fluidics, Phys. Rev. Appl. **11**, 014047 (2019).
[4] Z. Tan, M. Yang, and M. Ripoll, Microfluidic Pump Driven by Anisotropic Phoresis, Phys. Rev. Appl. **11**, 054004 (2019).
[5] A. J. Conde, A. Bianchetti, F. E. Veiras, A. Federico, J. M. Cabaleiro, M. Dufva, R. E. Madrid, and L. Fraigi, A polymer chip-integrable piezoelectric micropump with low backpressure dependence, RSC Adv. **5**, 49996 (2015).
[6] S. Litster, M. E. Suss, and J. G. Santiago, A two-liquid electroosmotic pump using low applied voltage and power, Sens. Actuators A: Phys. **163**, 311 (2010).
[7] A. J. McElrone, B. Choat, G. A. Gambetta, and C. R. Brodersen, Water uptake and transport in vascular plants, Nat. Educ. Knowledge **4**, 6 (2013).
[8] M. Lamb, G. W. Koch, E. R. Morgan, and M. W. Shafer, in *Proc. SPIE 9429, Bioinspiration, Biomimetics, and Bioreplication* (2015), Vol. 9429.
[9] M. Lee, H. Lim, and J. Lee, Fabrication of artificial leaf to develop fluid pump driven by surface tension and evaporation, Sci. Rep. **7**, 14735 (2017).
[10] T. Zhou, J. Yang, D. Zhu, J. Zheng, S. Handschuh-Wang, X. Zhou, J. Zhang, Y. Liu, Z. Liu, C. He, and X. Zhou, Hydrophilic sponges for leaf-inspired continuous pumping of liquids, Adv. Sci. **4**, 1700028 (2017).
[11] D. Juncker, H. Schmid, U. Drechsler, H. Wolf, M. Wolf, B. Michel, N. de Rooij, and E. Delamarche, Autonomous microfluidic capillary system, Anal. Chem. **74**, 6139 (2002).
[12] X. Wang, J. A. Hagen, and I. Papautsky, Paper pump for passive and programmable transport, Biomicrofluidics **7**, 14107 (2013).
[13] J. M. Li, C. Liu, Z. Xu, K. Zhang, X. Ke, and L. Wang, A microfluidic pump/valve inspired by xylem embolism and transpiration in plants, PLoS ONE **7**, 1 (2012).
[14] T. D. Wheeler and A. D. Stroock, The transpiration of water at negative pressures in a synthetic tree, Nature **455**, 208 (2008).
[15] V. M. Gunko, I. N. Savina, and S. V. Mikhalovsky, Properties of water bound in hydrogels, Gels **3**, 37 (2017).
[16] J. M. Li, C. Liu, K. P. Zhang, X. Ke, Z. Xu, C. Y. Li, and L. D. Wang, A micropump based on water potential difference in plants, Microfluid. Nanofluidics **11**, 717 (2011).
[17] H. Kim, K. Kim, and S. J. Lee, Compact and thermosensitive nature-inspired micropump, Sci. Rep. **6**, 36085 (2016).
[18] I. M. El-Sherbiny and M. H. Yacoub, Hydrogel scaffolds for tissue engineering: Progress and challenges, Glob. Cardiol. Sci. Pract. **2013**, 316 (2013).
[19] R. Crawford, T. E. Murphy, A. K. da Silva, and H. Berberoglu, Experimental characterization of the effects

of geometric parameters on evaporative pumping, Exp. Therm. Fluid Sci. **51**, 183 (2013).

[20] X. Noblin, L. Mahadevan, I. A. Coomaraswamy, D. A. Weitz, N. M. Holbrook, and M. A. Zwieniecki, Optimal vein density in artificial and real leaves, Proc. Natl. Acad. Sci. **105**, 9140 (2008).

[21] Y. Chen and P. Cheng, An experimental investigation on the thermal efficiency of fractal tree-like microchannel nets, Int. Commun. Heat Mass Transfer **32**, 931 (2005).

[22] T. ul Islam and P. S. Gandhi, Fabrication of multscale fractal-like structures by controlling fluid interface instability, Sci. Rep. **6**, 37187 (2016).

[23] C. V. Adake, P. Bhargava, and P. S. Gandhi, Effect of surfactant on dispersion of alumina in photo polymerizable monomers and their uv curing behavior for microstereolithography, Ceram. Int. **41**, 5301 (2015).

[24] See Supplemental Material at http://link.aps.org/supplemental/10.1103/PhysRevApplied.12.031002 for more details on structural characterization of the fractal channel network. The document also contains the derivation of Eq. (1) describing the steady-state configuration of the porous substrate and lists the values of different model parameters.

[25] M. Liu, J. Wu, Y. Gan, D. A. H. Hanaor, and C. Q. Chen, Evaporation limited radial capillary penetration in porous media, Langmuir **32**, 9899 (2016).

[26] D. Shou, L. Ye, and J. Fan, The fastest capillary flow under gravity, Appl. Phys. Lett. **104**, 231602 (2014).

[27] L. D. Landau and E. M. Lifshitz, *Fluid Mechanics* (Pergamon Press, Oxford, England, 1987), p. 247.

[28] S. Liu, Y. Zhang, and P. Liu, Heat transfer and pressure drop in fractal microchannel heat sink for cooling of electronic chips, Heat Mass Transfer **44**, 221 (2007).

[29] R. Arbteret al., Experimental determination of the permeability of textiles: A benchmark exercise, Compos. Part A: Appl. Sci. Manuf. **42**, 1157 (2011).

[30] S. Sharma and D. A. Siginer, Permeability measurement methods in porous media of fiber reinforced composites, Appl. Mech. Rev. **63**, 020802 (2010).

[31] C. Nie, A. J. H. Frijns, R. Mandamparambil, and J. M. J. den Toonder, A microfluidic device based on an evaporation-driven micropump, Biomed. Microdevices **17**, 47 (2015).

[32] Z.-R. Xu, C.-H. Zhong, Y.-X. Guan, X.-W. Chen, J.-H. Wang, and Z.-L. Fang, A microfluidic flow injection system for dna assay with fluids driven by an on-chip integrated pump based on capillary and evaporation effects, Lab Chip **8**, 1658 (2008).

[33] Y.-X. Guan, Z.-R. Xu, J. Dai, and Z.-L. Fang, The use of a micropump based on capillary and evaporation effects in a microfluidic flow injection chemiluminescence system, Talanta **68**, 1384 (2006).